Catena 122 (2014) 130–139

Contents lists available at ScienceDirect

Catena

journal homepage: www.elsevier.com/locate/catena

Characteristics of the fifth paleosol complex (S_5) in the southernmost part of the Chinese Loess Plateau and its paleo-environmental significance

Chuan-Qin Huang [a,b], Wen-Feng Tan [a,b,*], Ming-Kuang Wang [c], Luuk K. Koopal [d]

[a] State Key Laboratory of Soil Erosion and Dryland Farming on the Loess Plateau, Institute of Soil and Water Conservation, Chinese Academy of Sciences & Ministry of Water Resources, Yangling, Shaanxi 712100, PR China
[b] Key Laboratory of Arable Land Conservation (Middle and Lower Reaches of Yangtze River), Ministry of Agriculture, Huazhong Agricultural University, Wuhan, Hubei 430070, PR China
[c] Fujian Academy of Agricultural Sciences, Fuzhou 350003, PR China
[d] Laboratory of Physical Chemistry and Colloid Science, Wageningen University, Dreijenplein 6, 6703 HB Wageningen, The Netherlands

ARTICLE INFO

Article history:
Received 8 November 2013
Received in revised form 14 June 2014
Accepted 19 June 2014
Available online 18 July 2014

Keywords:
Chinese Loess Plateau
Clay mineral weathering
Paleosol
Pedogenesis
Pedogenic environment

ABSTRACT

The most prominent paleosol unit in the Chinese Loess Plateau (CLP) is the fifth paleosol complex (S_5) with its well-developed very thick and dark colored pedons. To provide more insight in the formation of S_5 and its environmental significance, the pedogenesis and clay mineral transformation in the S_5 of the Wugong section (Shaanxi Province) on the southernmost CLP are analyzed. S_5 at the Wugong section is essentially composed of three well-developed reddish pedons (i.e., $S_{5\text{-}1}$, $S_{5\text{-}2}$, $S_{5\text{-}3}$) which signify three glacial–interglacial climatic fluctuations during its formation. Complete decalcification in each pedon and a calcic horizon of only 30–50 cm in thickness beneath each of the three pedons suggests that after deposition the pedons developed with a relatively stable surface in a sustained warm and humid climate. Clay formation in the S_5 includes neogenesis of clay materials by in situ post-depositional weathering and mechanical migration of the fine fraction after complete decalcification.

Complete leaching of $CaCO_3$, intensive clay formation (with 60–100% higher clay content than that in the overlying and underlying loess (L_5 and L_6)) and extremely high magnetic susceptibility in the S_5 pedons reflected a warmer, more humid climate and soil environment for pedogenesis than in the 'optimum' Holocene. However, the chemical alteration of the phyllosilicate minerals was weak and restrained by the hard calcic horizon, the compact argillic horizon and the flat terrain. The major clay mineral weathering processes during the formation of the S_5 pedons at the Wugong section were depotassication, hydrolysis of primary minerals and degradation of chlorite. The pedogenesis in a loess–paleosol sequence and its pedogenic environment can best be deduced from combined data on pedogenic properties, and geochemical and mineralogical characteristics.

1. Introduction

Thick loess–paleosol sequences on the Chinese Loess Plateau (CLP) provide one of the most complete terrestrial records of the global paleoclimate and the Asian monsoon through the Quaternary period (Kukla, 1987). Loess is an eolian sediment deposited in a cold glacial period, while paleosol is the weathered equivalent of loess formed in a warm interglacial period. The loess–paleosol sequences on the CLP, reflect the balance between the accumulation rate of loess and the in situ pedogenesis after deposition controlled by the relative strength of the winter and summer monsoons (Liu, 1985). They have been developed as a consequence of this alternation between the dominance of the winter and summer monsoons that closely resemble the glacial–interglacial cycles represented by the oxygen-isotope compositions of foraminifera in deep sea sediments (Liu, 1985; Williams et al., 1988). Proxies such as grain size, magnetic susceptibility and geochemistry have been used for examining these climate changes (An et al., 1991a, b; Ding et al., 2001; Yang et al., 2006).

In most regions of the CLP the fifth paleosol (S_5) is a complex paleosol composed of three pedons, coded downwards as $S_{5\text{-}1}$, $S_{5\text{-}2}$ and $S_{5\text{-}3}$ (Han et al., 1998; Liu et al., 1990). Systematic correlations between marine oxygen-isotope curves and magnetic susceptibility variations of the loess–paleosol sequences suggest that S_5 developed from 0.62 to 0.48 Ma B.P., and was correlated with marine oxygen-isotope stages ($\delta^{18}O$) from 13 to 15 (correlative to the $S_{5\text{-}1}$, $S_{5\text{-}2}$ and $S_{5\text{-}3}$, respectively) (Heller and Evans, 1995; Kukla, 1987). The S_5, a record of climatic

* Corresponding author. Tel./fax: +86 27 87287508.
E-mail address: wenfeng.tan@hotmail.com (W.-F. Tan).

http://dx.doi.org/10.1016/j.catena.2014.06.009
0341-8162/

optimum during the last 1.2 Ma B.P., is the most prominent paleosol unit on the CLP, and it is characterized by its great thickness, reddish color, and well-developed clay coating (An et al., 1987). Pollen analysis in the S_5 paleosol of Xi'an and Baoji in Shaanxi Province, China has revealed that the vegetation assemblage was characterized by a combination of temperate broad-leafed trees (e.g., Quercus, Walnut and Basswood) and northern subtropical broad-leafed trees (e.g., Symplocos, Sweetgum and Pterocarya) (Zhao, 1994). Pollen evidence further signified a dominated forest landscape paleoecology and a northern subtropical condition for soil development in this region. However, based on paleo-rainfall amounts evaluated by using data of carbonate precipitation, Han et al. (1998) have suggested that in the Shijiawan and Chang'an sections located in the Guanzhong basin, grasslands dominated the paleovegetation during the development of $S_{5\text{-}1}$ and that the paleoclimatic conditions were perhaps even drier than at present (Han et al., 1998). This disparity on the paleoclimatic interpretation for S_5 is due to the different profiles studied and the limitations of the climatic indicators.

To obtain additional information, Huang et al. (2011) recently considered both paleoclimatic proxies and the mineralogical differentiation of the Holocene loess on the southernmost CLP to reveal the pedogenic environment and the pedogenesis. Mineralogical differentiation of loess and paleosol has occurred as result of eolian transportation and chemical weathering after deposition (Jeong et al., 2008, 2011). The various environmental conditions that prevailed during soil formation have determined the successive stages of the mineralogical evolution (Turpault et al., 2008). To further study the pedogenic processes and to better understand the changes of the paleoenvironment during the formation of S_5, the mineralogy and geochemistry of the clay fractions (<2 μm) of the S_5 on the southernmost CLP (Wugong section, Shaanxi Province) are analyzed and then correlated with paleoclimatic records such as, grain size, carbonate content and magnetic susceptibility. Field-observed profile characteristics of the paleosol complex in the Wugong section are consistent with the description of the S_5 in the Baoji section (Liu et al., 1990) which is 80 km to the west of the Wugong section. The Wugong section is part of a high platform and does not exhibit evidence of human perturbation or accelerated erosion. The Holocene paleosol (S_0) studied by Huang et al. (2011) and paleosol complex studied here are located at the same site of Wugong. According to ^{14}C dating of the Holocene paleosol (S_0) and field-observed consequence of loess-paleosol alternation, it can be confirmed that the paleosol complex studied is the fifth paleosol (S_5). With the comprehensive analysis together with field observations, more insight is gained in the evolution of S_5 over time and in the variations of the paleoenvironment during the formation of S_5.

2. Materials and methods

2.1. Field description and sampling

The Wugong section (N 34°19′17″, E 108°07′08″) is situated on the southernmost Chinese Loess Plateau (CLP), at an elevation of about 500 m a.s.l. (Fig. 1a). The present day average annual temperature and precipitation are 12–14 °C and 650–750 mm, respectively. The climate type of this region is a warm temperate semi-humid continental monsoon climate. In Chinese soil taxonomy, the modern zonal soil in this region is Eum-Orthic Anthrosols (Cooperative Research Group on Chinese Soil Taxonomy, 2001).

The fifth paleosol complex (S_5) is essentially composed of three well-developed reddish pedons ($S_{5\text{-}1}$, $S_{5\text{-}2}$, $S_{5\text{-}3}$ numbered downward) of 1.8, 1.8 and 1.5 m in thickness, respectively (Fig. 1b, c, d). The carbonate nodule horizons of 30–50 cm in thickness beneath the pedons can easily be recognized, making them useful as a stratigraphic marker between pedons (Fig. 1b, c, d). Profile characteristics of the field observations are summarized in Table 1. Vertically oriented samples were collected at 20 cm intervals from the $S_{5\text{-}1}$ and $S_{5\text{-}2}$, and at 10 cm intervals from the $S_{5\text{-}3}$. From the adjacent overlying and underlying loess (L_5 and L_6, respectively) four samples were taken at 20 cm intervals. Also from each of the three calcic horizons a sample was collected.

2.2. Analytical methods

2.2.1. Soil physicochemical properties

The samples were air dried, crushed and passed through a 0.25 mm sieve for soil magnetic susceptibility measurement and through a 2 mm sieve for carbonate content and particle-size distribution measurements. The magnetic susceptibility (M_S) was measured by a Bartington MS-2B susceptibility meter at low-frequency (0.47 kHz/χ_{lf}) and recorded in SI unit (10^{-8} m^3/kg) (Zhou et al., 1990). Soil calcium carbonate was determined by using the Chittick apparatus (Dreimanis, 1962). For further analysis the samples were pretreated for further analysis with acetic acid solution buffered with sodium acetate (pH = 5.0) to remove the calcium carbonate and with 10% H_2O_2 solution to remove organic matter. Suspensions were then washed several times with distilled water to remove excess ions and to assist dispersion of the clays. Silt and clay were separated from the sand fraction (2–0.05 mm) by wet-sieving through a 0.05 mm sieve. The silt fraction (0.05–0.002 mm) was separated from the clay fraction (<0.002 mm) by sedimentation under gravity (Gee and Bauder, 1986). The clay fraction was washed and centrifuged repeatedly with double deionized water and anhydrous alcohol to remove the excess salts. The sand, silt and concentrated clay fractions were dried and weighed to obtain the percent of each fraction.

The chemical composition of the selected clay samples was determined by wavelength dispersive X-ray fluorescence spectrometry (WD-XRF, PW4400) at the State Key Laboratory of Loess and Quaternary Geology of the Institute of Earth Environment, Chinese Academy of Sciences in Xi'an. To perform the analysis a 0.6 g clay sample was mixed with 6 g of dry lithium tetraborate ($Li_2B_4O_7$) and fused into a 32 mm diameter glass bead. Calibrations were done with 28 nationally certified reference materials of soil (GBW07401–GBW07416 and GBW07301–GBW07312). Analytical accuracy was checked by parallel analysis of two national standards (GSS-8 and GSD-12), and amounted to 1–2%.

2.2.2. Soil mineralogy

Mineralogical measurements of the clay fractions were carried out by X-ray diffraction (XRD). Prior to the XRD measurement free Fe-oxides and amorphous Al-phases were removed by dithionite–citrate–bicarbonate (DCB) extraction (Mehra and Jackson, 1960; He et al., 1994). For the XRD measurements specimens of the clay samples were saturated with magnesium (Mg) or with potassium (K) and mounted as slurries on glass slides. Air-dried Mg-saturated samples were analyzed at 25 °C after solvation in glycerol for 24 h (Mg–glycerol). Air-dried K-saturated samples were X-rayed at 25 °C before and after heating at 300 °C and 550 °C for 2 h (K-25 °C, K-300 °C, K-550 °C). Another specimen of clay was treated in 6 M HCl to remove possible chlorite and saturated with K and X-rayed at 25 °C (HCl-K). The 3° to 30° (2θ) range was scanned stepwise at a scanning speed of 1° (2θ) min^{-1} by using a Bruker D8 X-ray diffractometer (CuKα radiation generated with 40 kV accelerating potential and 40 mA tube current).

Identification of the clay minerals was based on the comparison of the XRD patterns obtained under the five different measurement conditions: Mg–glycerol, K-25 °C, K-300 °C, K-550 °C and HCl-K. Illite is recognized by its 1.0 nm peak in all treatments. Smectite is identified by the presence of a 1.8 nm peak in the Mg–glycerol sample and the absence of this peak in all K-saturated samples. Vermiculite is identified by the presence the 1.4 nm peak in the Mg–glycerol sample which is absent in the K-25 °C sample. Chlorite maintains a 1.4 nm peak after heat treatment of 2 h at K-550 °C. Kaolinite is identified by the presence of a peak at 0.71 nm in the

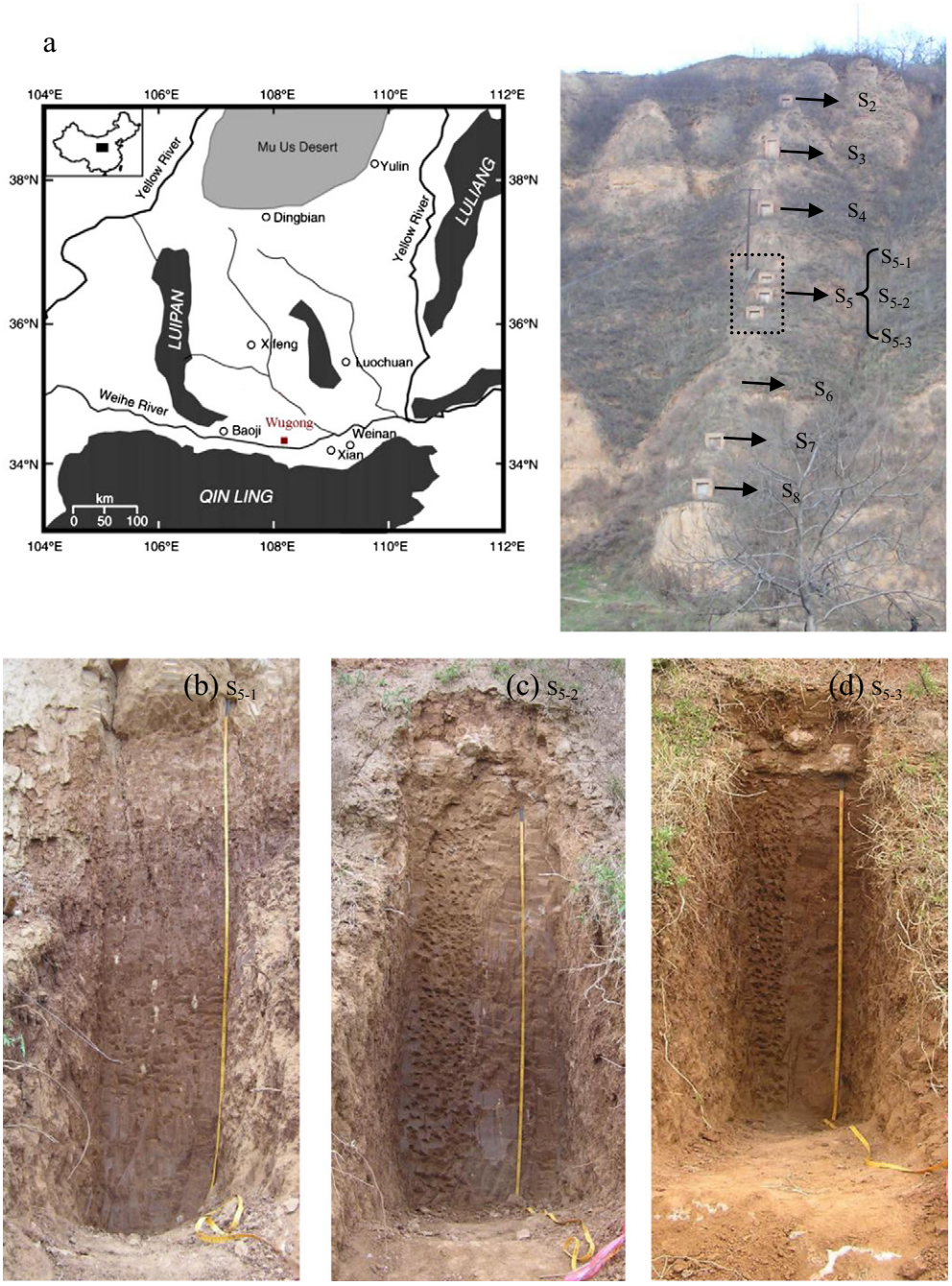

Fig. 1. Location and stratigraphy of the S_5 profile of the Wugong section. (a) Location of the Wugong; (b–d) profiles of the $S_{5\text{-}1}$, $S_{5\text{-}2}$ and $S_{5\text{-}3}$, respectively.

Mg–glycerol, K-25 °C, K-300 °C and HCl-K sample but the absence of this peak in the K-550 °C sample. Semi-quantitative estimates of the proportions of the clay minerals in the samples were derived from the integrated peak areas of the characteristic peaks (Pai et al., 1999). The relative percentages of illite, smectite, chlorite, vermiculite and kaolinite were determined using empirically estimated weighting factors (Biscaye, 1964; Brindley and Brown, 1980). Kaolinite and chlorite were identified by the presence of a peak at 0.71 nm and separated by the peaks at 0.358 nm (kaolinite, d(002)) and 0.354 nm (chlorite, d(004)) in the Mg–glycerol sample (Biscaye, 1964; Hillenbrand and Ehrmann, 2001).

3. Results

3.1. Soil chemical and physical characteristics

$CaCO_3$ in accumulated eolian dust is soluble and mobile and can be affected by pedogenetic processes (Gallet et al., 1996). Variations in

Table 1
Description of the fifth paleosol complex (S_5) in the Wugong section on the southernmost Loess Plateau, China.

Stratigraphic subdivisions	Thickness (cm)	Pedological description[b]
L_5	Overlying loess	Light yellowish-brown (10YR7/6)[a], silty clay loam, granular structure, firm, abundant fine bio-pores.
S_{5-1}	180	0–20 cm, light brown (7.5YR5/6), silty clay loam; 20–180 cm, reddish-brown (5YR4/6), silty clay. Prismatic structure, firm, a small quantity of pseudomycelium in the 0–40 cm horizon, small rusty and dark mottles disperse in the 40–80 cm horizon, abundant clay coating on the walls of soil pores and cracks in the middle and lower part.
Calcic horizon (30 cm)		
S_{5-2}	180	0–40 cm, yellowish-brown (10YR5/6), 40–80 cm, brown (7.5YR4/6), silty clay loam 80–180 cm, muddy reddish-brown (5YR4/4), 80–160 cm, silty clay. Prismatic structure, firm, abundant pseudomycelium in the 0–60 cm horizon, moderate clay coating in the lower part.
Calcic horizon (30 cm)		
S_{5-3}	150	0–20 cm, brown (7.5YR4/4), silty clay loam; 20–100 cm, muddy reddish-brown (5YR4/4), silty clay; 100–150 cm, brown (7.5YR4/6), silty clay loam. Prismatic structure, firm, moderate pseudomycelium in the 0–30 cm horizon.
Calcic horizon (50 cm)		
L_6	Underlying loess	Light yellowish-brown (10YR7/6), silty loam, granular structure, firm, moderate pseudomycelium, abundant fine bio-pores.

[a] Munsell soil color chart.
[b] Sand: 2–0.05 mm, silt: 0.05–0.002 mm, clay: <0.002 mm.

carbonate contents of the loess–paleosol layers are therefore the result of leaching and are indicative of the changes in precipitation and soil moisture during the dust accumulation and pedogenesis after deposition. The $CaCO_3$ content in each paleosol pedon (S_{5-1}, S_{5-2} and S_{5-3}) decreased with depth and reached the lowest level (approximately equal to zero) in the sub-horizon (Fig. 2a), which signified the intensive decalcification in the paleosol pedons. Dissolved carbonate was precipitated in the horizon beneath each paleosol pedon as indicated by the white and firm calcic horizon with a depth of 30–50 cm (Table 1 and Fig. 1) and extremely high $CaCO_3$ content varying between 35% and 55% (Fig. 2). By assuming that the carbonate content of least-weathered loess is about 10% (Liu, 1966), the 10–12% carbonate detected in the overlying loess (L_5) indicates a very scarce soil water reserve and high evaporation. The higher $CaCO_3$ content (15–20%) in the underlying loess (L_6) must be the result of a combination of sedimentation of eolian dust with plenty of carbonate during the glacial period plus post-pedogenic leaching from the S_{5-3} during the warmer and wetter paleoclimate.

The particle size distribution in the loess–paleosol sequence reflects the balance between accumulation rate of loess and in situ pedogenesis after deposition (Huang et al., 2011). The sand fraction of the fifth paleosol complex (S_5) and the adjoining loess layers (L_5 and L_6) in the Wugong section is relatively low (3–16%) and the clay and silt fractions are depicted in Fig. 2b and c, respectively. The S_5 pedons had a silty clay

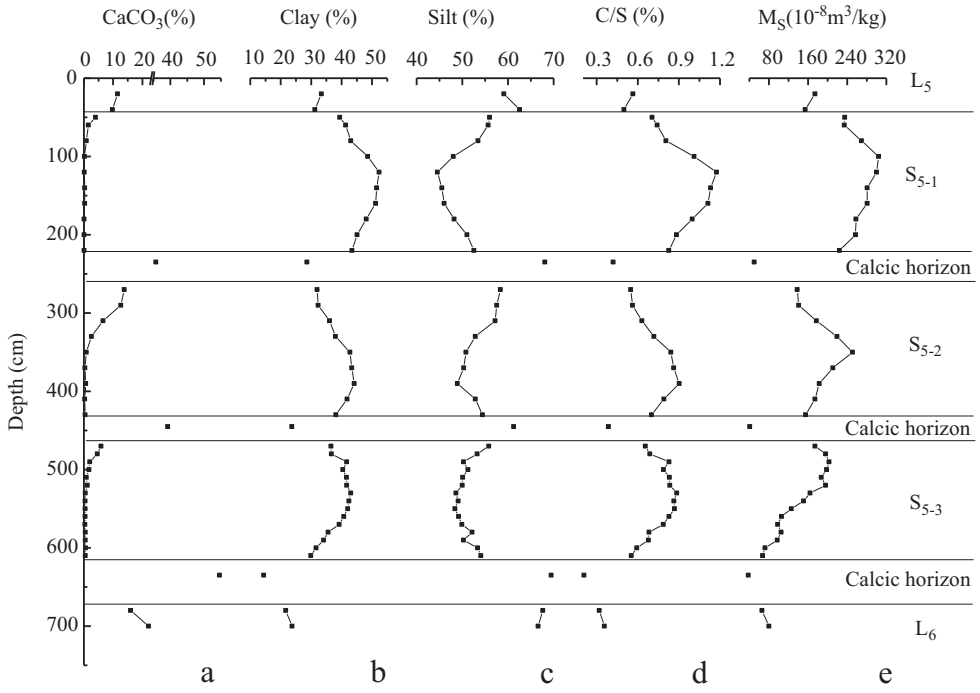

Fig. 2. $CaCO_3$ content, particle-size distribution, clay/silt ratio and magnetic susceptibility (M_S) of the L_5, S_5 and L_6 in the Wugong section on the southernmost Loess Plateau, China.

loam to silty clay texture with respectively, 43% to 57% silty grains (50–2 μm) and 30% to 53% clay grains (<2 μm). The overlying and underlying loess (L_5 and L_6) and calcic horizons had a silty loam or silty clay loam texture with dominated silty grains, ranging from 58% to 69% (Table 1 and Fig. 2b, c). The fine-grained paleosol pedons ($S_{5\text{-}1}$, $S_{5\text{-}2}$ and $S_{5\text{-}3}$) showed considerably higher clay contents than the loess layers (L_5 and L_6) and calcic horizons. In general, this implies that the paleosol pedons have undergone considerable weathering and pedogenesis in the warm and humid climate resulting in the large neoformation of fine grains.

In the pedon profiles, bowed trends in the silt and clay fraction curves were observed with a tendency of increasing clay content towards the subsoil (Fig. 2b, c). The clay content is maximized in the middle part of $S_{5\text{-}1}$ and $S_{5\text{-}3}$, and in the lower part of $S_{5\text{-}2}$. In general, a decrease in grain size is the result of the concomitant effects of weathering due to the physical breakdown of coarse particles and chemical neo-formation of clays. In the $S_{5\text{-}1}$ pedon the clay/silt ratio (Fig. 2d) reached the maximum value of 1.2, which signified more intensive clay formation in this pedon than in the $S_{5\text{-}2}$ and $S_{5\text{-}3}$ pedons with a maximum clay/silt ratio of no more than 0.9.

Magnetic susceptibility (M_S) is a measure of the concentration and categories of ultrafine-grained ferromagnetic minerals contained within the soil samples. The pedogenic origin is the prevailing hypothesis that accounts for the enhancement of magnetic susceptibility in loess and

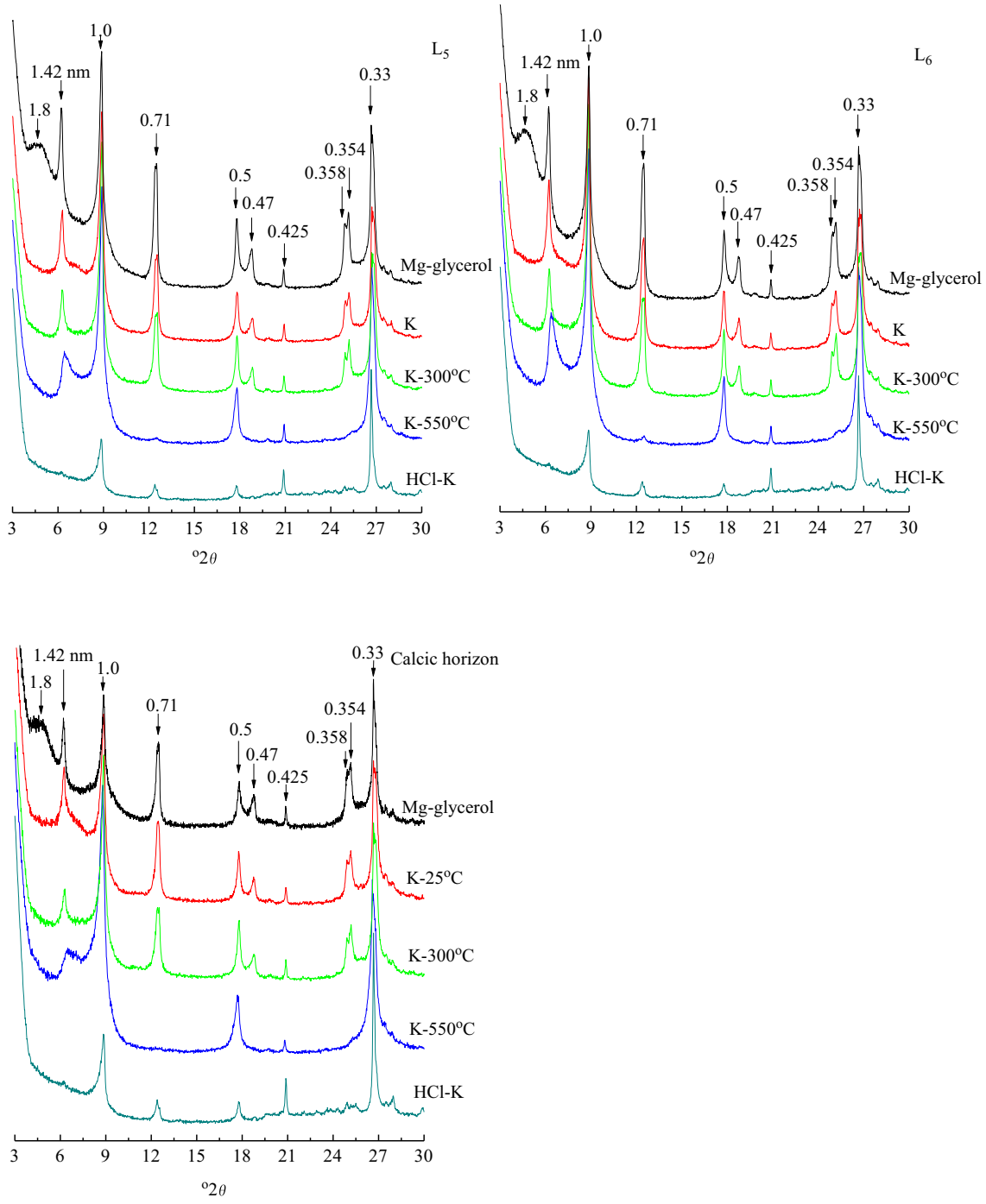

Fig. 3. XRD patterns (CuKα) with different treatments of oriented clay samples from the loess layers (L_5 and L_6) and calcic horizon in the Wugong section on the southernmost Loess Plateau, China.

paleosol (Zhou et al., 1990). The variation in M_S is therefore considered to be a record of the changes in intensity of pedogenesis, which result predominantly from precipitation changes related to the monsoonal climatic variation (An et al., 1991b). Magnetic susceptibility in each paleosol pedon first increased and then decreased gradually with depth. Overall, the magnetic susceptibility in each paleosol pedon (230–310 SI/10^{-8} m^3/kg, 130–260 SI/10^{-8} m^3/kg and 80–200 SI/10^{-8} m^3/kg for S_{5-1}, S_{5-2} and S_{5-3}, respectively) was higher than those in the overlying and underlying loess (L_5 and L_6) and calcic horizons, which signified a more intensive pedogenesis in the paleosol pedons than that in the loess layers and calcic horizon. The higher magnetic susceptibility of S_{5-1} than of S_{5-2} and S_{5-3} indicates that S_{5-1} had undergone more intensive pedogenesis than S_{5-2} and S_{5-3}. The lower magnetic susceptibility in the calcic horizons than in the L_5 and L_6 is due mainly to the dilution effect of the higher $CaCO_3$ content in the calcic horizons (Fig. 2a, e).

3.2. Composition of phyllosilicate minerals

The XRD patterns of the oriented clay samples from the L_5 and L_6 layers and the calcic horizons are depicted in Fig. 3. The broad peak around 1.8 nm in the Mg–glycerol XRD pattern was ascribed to the

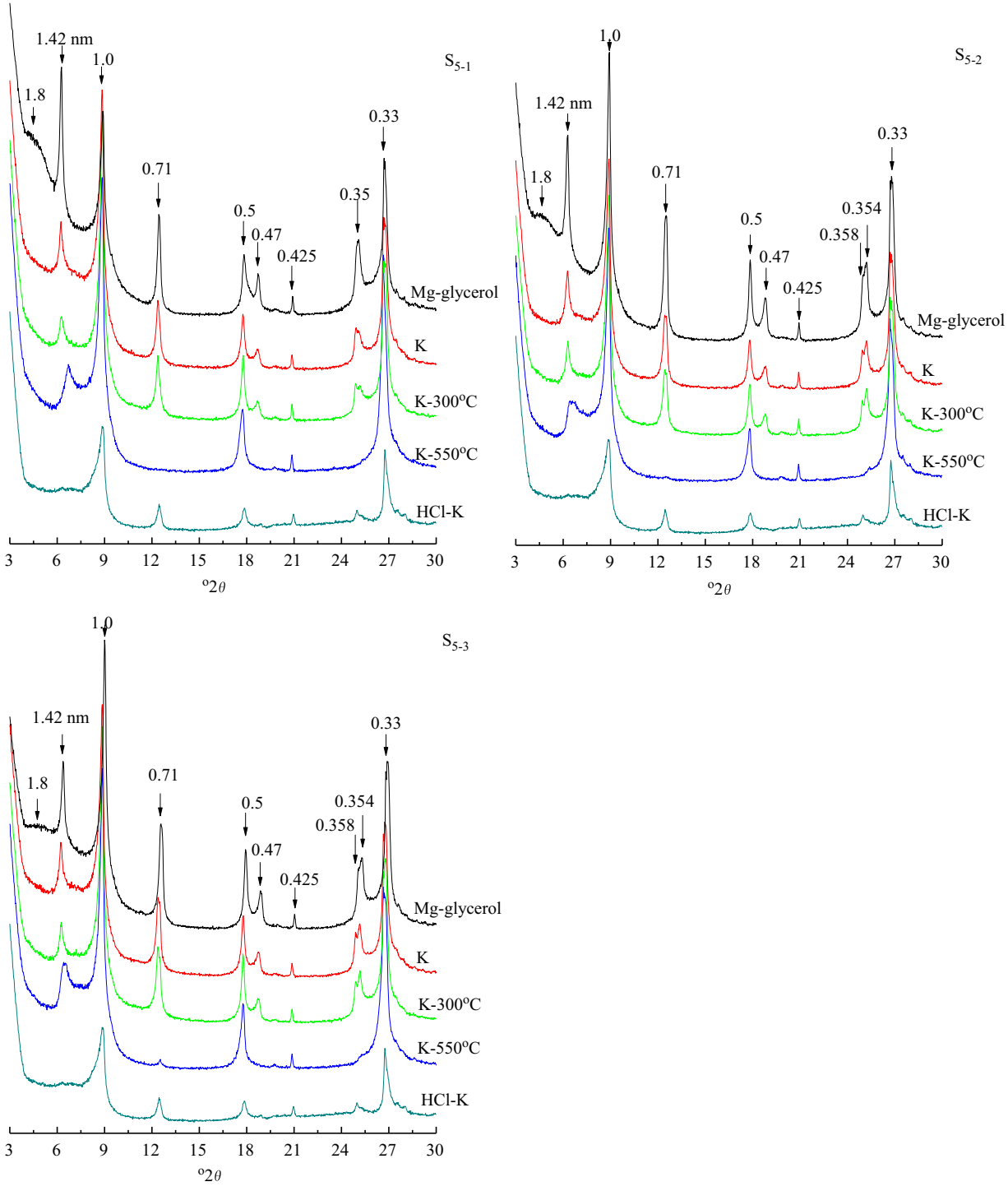

Fig. 4. XRD patterns (CuKα) with different treatments of oriented clay samples from the S_5 pedons in the Wugong section on the southernmost Loess Plateau, China.

presence of smectite and the intensive reflection peak at 1.0 nm peak in all the XRD patterns to illite. The 1.4 nm d-spacing peak was attributed to vermiculite and chlorite because this peak decreased and shifted to lower d-spacing resulting in an increasing intensity of the 1.0 nm reflection peak after K-25 °C and a peak at approximately 1.4 nm remained after K-550 °C. The XRD reflection peak at 0.71 nm was attributed to chlorite and/or kaolinite. The presence of the 0.71 nm peak in the HCl-K XRD pattern and its reduction after K-550 °C confirmed the presence of kaolinite. The XRD patterns illustrated that the major components of phyllosilicate assemblage in the L_5 and L_6 from the Wugong section were illite, chlorite, vermiculite, kaolinite and smectite. The XRD patterns of the oriented clay samples from the calcic horizons were comparable with those from L_5 and L_6 (Fig. 3) which implied the same phyllosilicate mineral composition in these layers.

In general, the XRD patterns of the oriented clay samples from the paleosol pedons (S_{5-1}, S_{5-2}, S_{5-3}) (Fig. 4) exhibited very similar changes with the five treatments throughout of the whole profile as those from the L_5 and L_6. However, close inspection of Figs. 3 and 4 showed that there was no visible reflection peak around 1.8 nm in the Mg–glycerol XRD patterns of the paleosol pedons (Fig. 4), which reflected the absence of well-crystallized smectite or a rare smectite that could not be detected in the paleosol pedons.

Semi-quantitative phyllosilicate compositions of the L_5, S_5 and L_6 stratums as a function of depth are summarized in Fig. 5. Illite (60–75%) was the dominant constituent. Chlorite (0–15%) and vermiculite (0–15%) contents were of secondary importance and Kaolinite (0–10%) and smectite (0–5%) contents were low. The illite content first increased with increasing depth and then decreased in deeper horizons of the paleosol pedons (S_{5-1}, S_{5-2}, S_{5-3}). The trends in variations of the chlorite content in the paleosol pedons were roughly opposite to the variations in illite content. Kaolinite and smectite contents in the clay fractions did not vary significantly with depth in the three paleosol pedons.

Table 2
Illite weathering characteristics (half height width (HHW), integral breath (IB), and chemical index of illite (ICI)) of the L_5, S_5 and L_6 in the Wugong section on the southernmost Loess Plateau, China.

Stratigraphic subdivisions	IC		ICI
	HHW (°Δ2θ)	IB (°Δ2θ)	
L_5	0.273 ± 0.006	0.459 ± 0.010	0.314 ± 0.043
S_{5-1}	0.320 ± 0.029	0.542 ± 0.048	0.333 ± 0.031
S_{5-2}	0.274 ± 0.005	0.483 ± 0.019	0.324 ± 0.037
S_{5-3}	0.278 ± 0.008	0.479 ± 0.022	0.297 ± 0.025
L_6	0.280 ± 0.023	0.492 ± 0.037	0.322 ± 0.018

3.3. Illite weathering

The illite weathering characteristics can be quantified by the 'illite crystallinity' (IC) and 'illite chemistry index' (ICI). The IC is composed of two values that characterize the 1.0 nm peak in the Mg–glycerol XRD patterns: the half height width (HHW) and integral breadth (IB) of the 1.0 nm peak. The IB is the width of the rectangle that has the same height and the same area as the measured peak (Ehrmann, 1998). The ICI is determined from the ratio of the areas of the peaks at 0.5 nm and 1.0 nm in the Mg–glycerol XRD patterns (Liu et al., 2005). Ratios below 0.5 represent Fe–Mg-rich illites, and ratios above 0.5 represent Al-rich illites (Liu et al., 2005). The obtained IC and ICI values are collected in Table 2. The average values of HHW and IB in the L_5, S_5 and L_6 stratums varied from 0.273 to 0.320 (°Δ2θ), and from 0.459 to 0.542 (°Δ2θ), respectively. The relatively high values of HHW and IB in the S_{5-1} pedon compared to those in the other subdivisions represent low illite crystallinity in the S_{5-1}. According to Ehrmann (1998), the low illite crystallinity is characteristic for a relatively intensive hydrolysis in humid and warm continental climate during the formation of S_{5-1}. The ICI values in the fifth paleosol complex (S_5) that varied between 0.297 and 0.333 were less than 0.50, which indicated that Fe–Mg-rich illite was observed. According to Liu et al. (2005), this also implied weak chemical weathering.

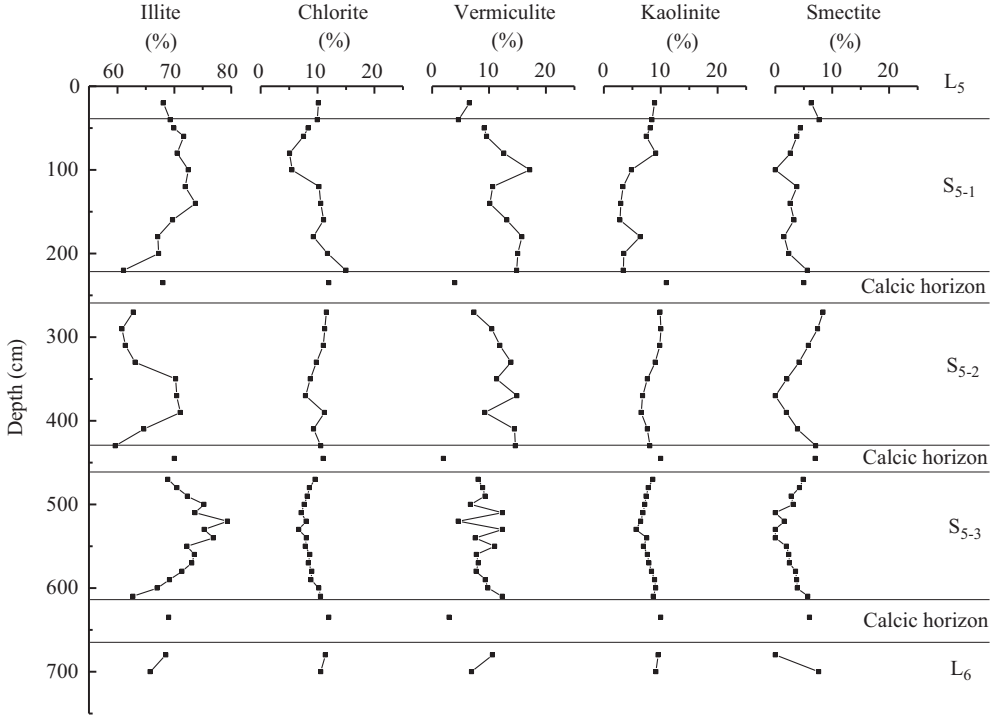

Fig. 5. Mineralogy in weight percent of the clay fraction from the L_5, S_5 and L_6 in the Wugong section on the southernmost Loess Plateau, China.

Table 3
Major elements as weight percent (wt. %) in the clay fraction (<2 μm) for selected samples of the L_5, S_5 and L_6 in the Wugong section on the southernmost Loess Plateau, China.

Stratigraphic subdivisions	Depth (cm)	SiO_2	Al_2O_3	Fe_2O_3[a]	LOI	SiO_2/Al_2O_3	SiO_2/R_2O_3[b]
L_5	20	42.25	19.97	9.03	12.91	4.00	3.03
S_{5-1}	100	49.29	22.05	10.68	8.27	3.80	2.90
	140	50.05	22.70	10.74	8.4	3.75	2.88
S_{5-2}	330	49.94	21.93	10.92	5.36	3.87	2.94
	350	48.51	21.56	10.85	8.06	3.83	2.90
S_{5-3}	500	48.60	21.89	10.72	8.08	3.77	2.88
	530	47.85	22.04	10.61	8.65	3.69	2.82
L_6	700	40.32	16.79	8.15	15.42	4.08	3.12

LOI: Loss on ignition at 1000 °C.
LOI: Loss on ignition at 1000 °C.
[a] Total Fe as Fe_2O_3.
[b] $R_2O_3 = Al_2O_3 + Fe_2O_3$.

3.4. Geochemical characteristics

Chemical compositions of the clay fractions of the paleosol pedons (S_{5-1}, S_{5-2} and S_{5-3}) and the loess layers (L_5 and L_6) as determined by XRF are summarized in Table 3. Consistent with the mineralogy, the chemical composition of the clay fraction was dominated by SiO_2 (40–50%), Al_2O_3 (16–23%) and Fe_2O_3 (8–11%). Al_2O_3 and Fe_2O_3 were approximately 15–30% higher in the S_5 pedons than in the L_5 and L_6, indicating that the S_5 pedons had undergone stronger chemical weathering and leaching under the warmer and wetter paleoclimate and the more acidic environment. The molecular ratios of SiO_2/Al_2O_3 and $SiO_2/(Al_2O_3 + Fe_2O_3)$ (Table 3) serve as indicators of the chemical weathering of the silicate minerals. The lower ratios in the S_5 pedons than in the L_5 and L_6 also implied relatively intensive desilication in the S_5.

4. Discussion

4.1. Decalcification and paleo-rainfall

Calcium carbonate in the paleosol pedons (S_{5-1}, S_{5-2}, S_{5-3}) was intensively leached (Fig. 2), and dissolved carbonate was precipitated beneath S_{5-1}, S_{5-2} and S_{5-3}, as indicated by the hard white calcic horizons (Fig. 1, Table 1). This illustrates that the paleosol pedons (S_{5-1}, S_{5-2}, S_{5-3}) have experienced intensive decalcification which is characteristic for high paleo-rainfall during the paleosol-forming process. The calcic horizons of 30–50 cm in thickness for S_{5-1}, S_{5-2}, S_{5-3} indicate that after deposition the pedons developed with a relatively stable surface in a sustained warm and humid climate. In other words, the fifth paleosol complex (S_5) signifies three glacial–interglacial climatic fluctuations during the formation of S_5.

Although the weakly developed paleosol is alkaline at the beginning of the pedogenesis after eolian deposition, the eluviation and precipitation of carbonate could also happen at this condition (Zhao, 1994). The mineralogical composition of carbonate nodules collected from the CLP is mainly calcite together with some primary silicate minerals such as quartz, plagioclase, orthoclase and illite (Yang et al., 2013a). It can be speculated that eluviation and precipitation of carbonate occurred in the early stage of the pedogenesis and that these processes were just transient in the whole pedogenesis history. The $CaCO_3$ content in the sub-horizon of S_{5-1}, S_{5-2} and S_{5-3} was approximately equal to zero (Fig. 2a), which signified the complete decalcification in the paleosol pedons. Hence, it can be concluded that the eluviation and precipitation of carbonate did not last for the whole pedogenesis. In general, one should be very careful when quantitatively evaluating paleo-rainfall amounts for a paleosol by using data of carbonate precipitation since the conclusion based on precipitated carbonate, that the climate condition for the S_{5-1} located in the Guanzhong basin on the southernmost part of the CLP was even drier than at present (Han et al., 1998) is debatable.

A paleosol unit, referred to as vermiculated red soil (VRS), which is correlative to the S_4 and S_5 paleosol units on the CLP and to the marine oxygen-isotope stages 11–15 (Jiang et al., 1997; Qiao et al., 2003; Yin and Guo, 2006), is widely distributed in the region south of the Yangtze River. Formation of the white vein in the VRS primarily correlates with the development of S_{5-1} and implies a Mid-Pleistocene extreme East Asian summer monsoon (Yin and Guo, 2006). During the warmest and wettest climate span of 2.5 Ma when S_5 was formed, the Qinling Mountains lost their function as a climatic boundary between the subtropical and temperate zones of East Asia (Zhao et al., 2013). The moist summer air masses could cross the Qinling Mountains and reach the Guanzhong Plain where they led to high precipitation. Paleopedological, geochemical and magnetic susceptibility data from Xifeng, Changwu and Weinan sections (Guo et al., 1998) and analysis of dark red-brown lumpy ferruginous argillans (LFAs) (Zhao et al., 2013) and pollen (Zhao, 1994), all suggest that while the S_5 developed a subtropical climate prevailed on the southern Loess Plateau with a higher mean annual temperature (by 4–6 °C) and higher rainfall (by 200–500 mm) than at present.

4.2. Clay transformation and translocation

In general, clay enrichment due to soil formation in a humid climate, can act as an index of the effect of the summer monsoon on the pedogenesis intensity. The early weathering stage of the quaternary loose sediment is accompanied by chemical weathering as there is no physical weathering on the rock breaking and the refinement of coarse grain materials. This chemical weathering strengthened the clay formation in loess–paleosol sequences (Gong, 1992). The average clay content in the three pedons was 60–100% higher than that in the overlying and underlying loess (L_5 and L_6). This reflects not only the decreased effect of the winter monsoon on particle sorting of the eolian deposits, but also the intensified in situ clay neogenesis after deposition (Huang et al., 2011). Comparison of the particle analysis and clay/silt ratio results obtained for the S_5 pedons and the Holocene paleosol (S_0) in the Wugong section (Fig. 2 and Huang et al., 2011, Fig. 2) reveals a more intense process of clay formation in the S_5 pedons than in the Holocene paleosol (S_0). It can therefore be deduced that warmer and wetter climate conditions and soil environment have occurred in the period of the development and evolution of the S_5 pedons than during the 'optimum' Holocene.

Laboratory data-indicated peaks for clay fractions of the three paleosol pedons (S_{5-1}, S_{5-2}, S_{5-3}) and field-observed clay coatings on ped-faces, together with carbonate leaching and accumulation within each pedon indicate material translocation within S_5 (Fig. 2, Table 1). Mechanical migration (translocation) of clays can occur easily when decalcification is complete (Birkeland, 1974). Generally, the middle and lower horizons of the S_{5-1}, S_{5-2} and S_{5-3} were largely free of carbonate, which signified complete decalcification, and hence the translocation of clays in the S_5 pedons downwards in the profile was possible. It can conclude that clay formation in the S_5 pedons included neogenesis of clay materials by in situ post-depositional weathering and fine fraction mechanical migration.

4.3. Mineral weathering

Clay minerals in the fifth paleosol complex (S_5) and the overlying and underlying loess (L_5 and L_6) were dominated by illite with different amounts of chlorite, vermiculite, smectite and kaolinite throughout the profiles (Fig. 5). Inferring from the comparable mineral compositions, the parent materials throughout the profiles (L_5, S_5 and L_6) should also be comparable and have similar initial mineralogical composition. Compared to the loess horizons (L_5 and L_6) chlorite in the three paleosol pedons (S_{5-1}, S_{5-2}, S_{5-3}) decreased, while illite increased. However, the increase in illite (10%) was larger than the decrease in chlorite (Fig. 5) which reflects not only the transformation of chlorite, but also the weathering of the primary minerals (e.g. mica, feldspar) (Jeong et al., 2008) into illite in the S_5 pedons. This implies intensive mineral weathering and soil evolution due to the enhanced physical, chemical and biological weathering under the humid and warm climate during the development of the S_5 pedons. This is in accordance with the illite weathering characteristics and chemical composition (the relative higher illite chemistry index and the lower illite crystallinity and SiO_2/R_2O_3 ratio in the S_5 pedons than in the L_5 and L_6) (Tables 2 and 3). As the main iron-bearing silicate mineral, the weathering of chlorite provided free iron for the production of nanoscale Fe-oxides in the pedogenic process (Yang et al., 2013b). These Fe-oxides are responsible for the enhancement of the magnetic susceptibility signal in the S_5 pedons (Fig. 2e). Only trace amounts of smectite were detected in the profiles and absent in the paleosol pedons (Fig. 5) due to the increase in base leaching by the increased precipitation. Small amounts of kaolinite were found throughout the profile and the amounts were not subjected to any recognizable trends in the distribution (Fig. 5). The occurrence of smectite and kaolinite in the less weathered loess layers (L_5 and L_6) gives reason to believe that they are not newly formed within the profile, but originated from previously weathered source material transported from the northwestern arid inland deserts.

A similar composition of phyllosilicates was found in the Holocene paleosol (S_0) in the Wugong section on the CLP (Huang et al., 2011). Compared with the S_0, complete leaching of $CaCO_3$, intensive clay formation (i.e., in situ clay neogenesis after deposition and mechanical translocation of clays) and extremely high magnetic susceptibility in the S_5 pedons suggests a more intensive pedogenesis under the warmer and more humid climate and soil environment than in the optimum stage of the Holocene. However, the chemical weathering intensity in the S_5 pedons was approximately similar to that in the S_0 as reflected by the similar SiO_2/R_2O_3 ratios. These ratios varied from 2.82 to 2.94 in the S_5 pedons (Table 3), and from 2.84 to 3.02 in the S_0 (Huang et al., 2011, Fig. 3). There are three reasons that can explain this contradiction. (1) The S_5 pedons have a lower permeability than Holocene paleosol because of their fine grain-size composition (Fig. 2) and firm structure (Table 1) with a higher bulk density (1.65 to 1.70 g/cm^3, unpublished data). (2) The S_5 contains hard calcic horizons of 30–50 cm in thickness beneath the paleosol pedons (S_{5-1}, S_{5-2}, S_{5-3}), which were formed at the early stage of pedogenesis and these calcic layers could act as an 'aquifuge' to block element leaching out of the paleosol pedons. (3) The Wugong section was part of a high platform long before the formation of S_5 of great depth, and the low gradient of the platform probably led to only a small interflow and concomitant element leaching. Together, the hard calcic horizon, the compact argillic horizon and the flat terrain reduced the permeability of the S_5 and limited loss of alkali and alkaline earth elements from the parent materials, consequently mineral weathering was inhibited.

5. Conclusions

The fifth paleosol complex (S_5) in the Wugong section on the southernmost Chinese Loess Plateau (CLP) is basically composed of three thick and well-developed reddish pedons (S_{5-1}, S_{5-2}, S_{5-3}). The three pedons signify three glacial–interglacial climatic fluctuations during the formation of S_5. After deposition the S_{5-1}, S_{5-2} and S_{5-3} developed with a relatively stable surface in a sustained warm and humid climate. This could be concluded from the complete decalcification in each pedon and the calcic horizons of only 30–50 cm in thickness beneath each of the pedons. The complete decalcification in each pedon makes translocation of clays easy. Clay formation in the S_5 pedons therefore includes not only neogenesis of clay materials by in situ post-depositional weathering, but also fine fraction mechanical migration.

Complete leaching of $CaCO_3$, intensive clay formation and extremely high magnetic susceptibility in the S_5 pedons signified a more intensive pedogenesis under a warmer and more humid climate and soil environment than during the 'optimum' Holocene. However, chemical alteration of phyllosilicate minerals was weak due to the reduced permeability of the S_5 and the limited loss of alkali and alkaline earth elements from parent materials resulted from the hard calcic horizon, the compact argillic horizon and the flat terrain. The major clay mineral weathering processes for soil-formation of the S_5 in the Wugong profile were depotassication and hydrolysis of primary minerals and degradation of chlorite.

Acknowledgments

Financial support for this research came from the National Natural Science Foundation of China (41201230), the Open Program of the State Key Laboratory of Soil Erosion and Dryland Farming on the Loess Plateau, Institute of Soil and Water Conservation, CAS&MWR (K318009902-1301) and the One Hundred Elitist Program of Chinese Academy of Sciences (K318009902-281). The authors are grateful to Dr. N. Liu and F. Y. Li for soil sampling, to Dr. W. Zhao for the part of the laboratory work and to F. Wu for laboratory assistance.

References

An, Z.S., Liu, T.S., Zhu, Y.Z., Sun, F.Q., Ding, Z.L., 1987. The paleosol complex S5 in the China Loess Plateau — a record of climatic optimum during the last 1.2 Ma. GeoJournal 15, 141–143.
An, Z.S., Kukla, G., Porter, S.C., Xiao, J.L., 1991a. Late Quaternary dust flow on the Chinese Loess Plateau. Catena 18, 125–132.
An, Z.S., Kukla, G.J., Porter, S.C., Xiao, J.L., 1991b. Magnetic susceptibility evidence of monsoon variation on the Loess Plateau of Central China during the last 130,000 years. Quat. Res. 36, 29–36.
Birkeland, P.W. (Ed.), 1974. Pedology, Weathering, and Geomorphological Research. Oxford University Press, Oxford, pp. 103–124.
Biscaye, P.E., 1964. Distinction between kaolinite and chlorite in recent sediments by X-ray diffraction. Am. Mineral. 49, 1281–1289.
Brindley, G.W., Brown, G. (Eds.), 1980. Crystal structures of clay minerals and their x-ray identification. Mineralogical Society, Monogr., No.5, p. 495 (London).
Cooperative Research Group on Chinese Soil Taxonomy, Cooperative Research Group on Chinese Soil Taxonomy (Eds.), 2001. Chinese Soil Taxonomy. Science Press, Beijing New York, pp. 85–88.
Ding, Z.L., Yang, S.L., Sun, J.M., Liu, T.S., 2001. Iron geochemistry of loess and red clay deposits in the Chinese Loess Plateau and implications for long-term Asian monsoon evolution over the last 7.0 Ma. Earth Planet. Sci. Lett. 185, 99–109.
Dreimanis, A., 1962. Quantitative gasometric determination of calcite and dolomite by using Chittick apparatus. J. Sediment. Petrol. 32, 520–529.
Ehrmann, W., 1998. Implications of late Eocene to early Miocene clay mineral assemblages in McMurdo Sound (Ross Sea, Antarctica) on paleoclimate and ice dynamics. Palaeogeogr. Palaeoclimatol. Palaeoecol. 139, 213–231.
Gallet, S., Jahn, B.M., Torii, M., 1996. Geochemical characterization of the Luochuan loess–paleosol sequence, China, and paleoclimatic implications. Chem. Geol. 133, 67–88.
Gee, G.W., Bauder, J.W., 1986. Particle-size analysis, In: Klute, A. (Ed.), Methods of Soil Analysis. Part 1, Physical and Mineralogical Methods, 2nd ed. Agron. Monogr., 9. ASA and SSSA, Madison, WI, pp. 383–411.
Gong, Z.T. (Ed.), 1992. Change of Soil Environment. China Science & Technology Press, Beijing, p. 122 (In Chinese).
Guo, Z.T., Liu, T.S., Fedoroff, N., Wei, L.Y., Ding, Z.L., Wu, N.Q., Lu, H.Y., Jiang, W.Y., An, Z.S., 1998. Climate extremes in Loess of China coupled with the strength of deep-water formation in the North Atlantic. Glob. Planet. Chang. 18, 113–128.
Han, J.T., Fyfe, W.S., Longstaffe, F.J., 1998. Climatic implications of the S5 palaeosol complex on the Southernmost Chinese loess plateau. Quat. Res. 50, 21–33.
He, J.Z., Li, X.Y., Liu, F., Xu, F.L., 1994. Free Al-phrases in soil. Chin. Sci. Bull. 39 (5), 1426–1428 (In Chinese).
Heller, F., Evans, M.E., 1995. Loess magnetism. Rev. Geophys. 33, 211–240.
Hillenbrand, C.D., Ehrmann, W., 2001. Distribution of clay minerals in drift sediments on the continental rise west of the Antarctic Peninsula, ODP Leg 178, Sites 1095 and

1096. In: Barker, P.F., et al. (Eds.), Proceedings of the Ocean Drilling Program. Scientific Results, 178, pp. 1–29.
Huang, C.Q., Zhao, W., Liu, F., Tan, W.F., Koopal, L.K., 2011. Environmental significance of mineral weathering and pedogenesis of loess on the southernmost Loess Plateau, China. Geoderma 163, 219–226.
Jeong, G.Y., Hillier, S., Kemp, R.A., 2008. Quantitative bulk and single-particle mineralogy of a thick Chinese loess–paleosol section: implications for loess provenance and weathering. Quat. Sci. Rev. 27, 1271–1287.
Jeong, G.Y., Hillier, S., Kemp, R.A., 2011. Changes in mineralogy of loess–paleosol sections across the Chinese Loess Plateau. Quat. Res. 75, 245–255.
Jiang, F.C., Wu, X.H., Xiao, H.G., Zhao, Z.Z., Wang, S.M., Xue, B., 1997. Age of the vermiculated red soil in Jiujiang area, central China. J. Geomech. 3 (4), 27–32 (In Chinese).
Kukla, G., 1987. Loess stratigraphy in central China. Quat. Sci. Rev. 6, 191–219.
Liu, T.S. (Ed.), 1966. The Composition and Texture of Loess. China Science Press, Beijing (In Chinese).
Liu, T.S. (Ed.), 1985. Loess and the Environment. China Science Press, Beijing (In Chinese).
Liu, X.M., Liu, T.S., Heller, F., Xu, T.C., 1990. Frequency-dependent susceptibility of loess and quaternary paleoclimate. Quat. Sci. 1, 42–50 (In Chinese).
Liu, Z.F., Colin, C., Trentesaux, A., Blamart, D., 2005. Clay mineral records of East Asian monsoon evolution during late Quaternary in the southern South China Sea. Sci. China Ser. D Earth Sci. 48, 84–92.
Mehra, O.P., Jackson, M.L., 1960. Iron oxides removed from soils and clays by dithionite–citrate system buffered with sodium bicarbonate. Clay Clay Miner. 7, 317–327.
Pai, C.W., Wang, M.K., Wang, W.M., Houng, K.H., 1999. Smectites in iron-rich calcareous soil and black soils of Taiwan. Clay Clay Miner. 47, 389–398.
Qiao, Y.S., Guo, Z.T., Hao, Q.Z., Wu, W.X., Jiang, W.Y., Yuan, B.Y., Zhang, Z.S., Wei, J.J., Zhao, H., 2003. Loess–soil sequence in southern Anhui province: magnetostratigraphy and paleoclimatic significance. Chin. Sci. Bull. 48 (13), 1465–1469.
Turpault, M.P., Righi, D., Uterano, C., 2008. Clay minerals: precise markers of the spatial and temporal variability of the biogeochemical soil environment. Geoderma 147, 108–115.
Williams, D.F., Thunell, R.C., Tappa, E., Rio, D., Raffi, I., 1988. Chronology of the Pleistocene oxygen isotope record: 0–1.88 m.y. B.P. Palaeogeogr. Palaeoclimatol. Palaeoecol. 64, 221–240.
Yang, S.L., Ding, F., Ding, Z.L., 2006. Pleistocene chemical weathering history of Asian arid and semi-arid regions recorded in loess deposits of China and Tajikistan. Geochim. Cosmochim. Acta 70, 1695–1709.
Yang, S.L., Ding, Z.L., Gu, Z.Y., 2014. Acetic acid-leachable elements in pedogenic carbonate nodules and links to the East-Asian summer monsoon. Catena 117, 73–80.
Yang, T.S., Hyodo, M., Zhang, S.Y., Maeda, M., Yang, Z.Y., Wu, H.C., Li, H.Y., 2013b. New insights into magnetic enhancement mechanism in Chinese paleosol. Palaeogeogr. Palaeoclimatol. Palaeoecol. 369, 493–500.
Yin, Q.Z., Guo, Z.T., 2006. Mid-Pleistocene vermiculated red soils in southern China as an indication of unusually strengthened East Asian monsoon. Chin. Sci. Bull. 51 (2), 213–220.
Zhao, J.B. (Ed.), 1994. Quaternary Soils and Environment in Loess Area in North-western China. Scientific and Technological Press, Shaanxi, Xi'an (In Chinese).
Zhao, J.B., Cao, J.J., Jin, Z.D., Xiang, S., Shao, T.J., 2013. The fifth paleosol layer in the southern part of China's Loess Plateau and its environmental significance. Quat. Int.. http://dx.doi.org/10.1016/j.quaint.2012.12.044.
Zhou, L.P., Oldfield, F., Wintle, A.G., Robinson, S.G., Wang, J.T., 1990. Partly pedogenic origin of magnetic variations in Chinese loess. Nature 346, 737–739.